

Trends and projection of heavy snowfall in Hokkaido, Japan as an application of self- organizing map

Inatsu, Masaru
Faculty of Science, Hokkaido University

Kawazoe, Sho
Faculty of Science, Hokkaido University

Mori, Masato
Research Institute for Applied Mechanics, Kyushu University

<https://hdl.handle.net/2324/7177966>

出版情報 : Journal of Applied Meteorology and Climatology. 60 (10), pp.1483-1494, 2021-10-15.
American Meteorological Society
バージョン :
権利関係 : ©2021 American Meteorological Society



Trends and Projection of Heavy Snowfall in Hokkaido, Japan, as an Application of Self-Organizing Map

MASARU INATSU,^a SHO KAWAZOE,^b AND MASATO MORI^c

^a Faculty of Science and Research Center for Integrative Natural Hazard Mitigation, Hokkaido University, Sapporo, Japan

^b Faculty of Science, Hokkaido University, Sapporo, Japan

^c Research Institute for Applied Mechanics, Kyushu University, Kasuga, Fukuoka, Japan

(Manuscript received 5 May 2021, in final form 13 September 2021)

ABSTRACT: This paper showed the frequency of local-scale heavy winter snowfall in Hokkaido, Japan, its historical change, and its response to global warming using self-organizing maps (SOM) of synoptic-scale sea level pressure anomaly. Heavy snowfall days were here defined as days on which the snowfall exceeded 10 mm in water equivalent. It was shown that the SOMs can be grouped into three categories for heavy snowfall days: 1) a passage of extratropical cyclones to the south of Hokkaido, 2) a pressure pattern between the Siberian high and the Aleutian low, and 3) a low pressure anomaly just to the east of Hokkaido. Groups 1 and 2 were associated with heavy snowfall in Hiroo (located in southeastern Hokkaido) and in Iwamizawa (western Hokkaido), respectively, and heavy snowfall in Sapporo (western Hokkaido) was related to group 3. The large-ensemble historical simulation reproduced the observed increasing trend in group 2, and future projections revealed that group 2 was related to a negative phase of the western Pacific pattern and that the frequency of this group would increase in the future. Heavy snowfall days associated with SOM group 2 would also increase as a result of the increase in water vapor and preferable weather patterns in a globally warming climate, in contrast to the decrease of heavy snowfall days at other sites associated with SOM group 1.

KEYWORDS: Asia; Synoptic climatology; Snowfall; Winter/cool season; Climate prediction; Ensembles; Trends; Neural networks

1. Introduction

The climate of Hokkaido Island, Japan (Fig. 1a), is characterized by abundant snowfall in winter. According to the 60-yr observation by the Japan Meteorological Agency (JMA), 90%-, 95%-, and 99%-tile values of daily snowfall are ~5, ~10, and ~20 mm in water equivalent, respectively (Table 1). The spatial distribution of the number of heavy snowfall days, defined in this paper as days when snowfall exceeds 10 mm in water equivalent (Fig. 1a), strongly depends on synoptic weather patterns around Hokkaido (Fig. 1b). A high meridional temperature gradient zone during the winter season allows extratropical cyclones to develop rapidly due to linear baroclinic instability (Lindzen and Farrell 1980). Explosively deepening extratropical cyclones (Sanders and Gyakum 1980; Yoshida and Asuma 2004; Iwao et al. 2012) often result in heavy snow, blowing snow, high tides, and gale-force winds in southeastern Hokkaido. Although heavy snowfall is infrequent in this region, it often occurs from the southern passage of extratropical cyclones. In contrast, the climatological wind is northwesterly over Hokkaido because of a quasi-stationary pressure gradient between the Siberian high (H located in northwestern China in Fig. 1b) and the Aleutian low (L in the western North Pacific). This northwest wind brings extremely cold air across the relatively warm ocean, and the resulting heat and moisture fluxes form convective snowbands (Tsuboki et al. 1989). These snowbands can bring heavy snowfall to the coastal and inland areas of western Hokkaido, but their location is

highly sensitive to changes in the wind direction, which is related to a slight change of pressure patterns from climatology (Tachibana 1995). Wind speed also plays an important role in determining the inland extent of snowbands (Veals et al. 2019, 2020). Some mesoscale factors that influence distribution of the snowbands over Hokkaido include the terrain configuration of the Russian coast (Ohtake et al. 2009) and deflection, channeling, and convergence induced by the terrain in Hokkaido (Fujiyoshi et al. 1992; Campbell et al. 2018).

Kawazoe et al. (2020) effectively applied self-organizing maps (SOMs), proposed by Kohonen (1995), to classify typical weather patterns related to heavy snowfall in Sapporo (S in Fig. 1a), located on the western side of Hokkaido. They found, in the 5-km dynamical downscaling result (Hoshino et al. 2020) from the database for Policy Decision-Making for Future climate change (d4PDF; Mizuta et al. 2017), that patterns producing the highest number of heavy snow events are identified as days with a strong low pressure anomaly to the east to northeast of the Hokkaido, low pressure anomaly over central Japan, or moderately strong high pressure anomaly over the Siberian continent, similar to results by Tachibana (1995). Tanji et al. (2021) adopted methods from Kawazoe et al. (2020) create a hazard map of blowing snow over Hokkaido by utilizing the SOMs based on the reanalysis data from 1960 to 2020. The SOM originally relocates uniform grid points in the (resolved) state space to be fit with the probability density function (PDF) of training data on the space, so that a cluster of SOM nodes can be regarded as an attractor of the dynamical system. If an unresolved phenomenon (heavy snowfall) is linked with resolved states (synoptic-scale environment), the SOM analysis can then diagnose the occurrence of unresolved

Corresponding author: Masaru Inatsu, inaz@sci.hokudai.ac.jp

DOI: 10.1175/JAMC-D-21-0085.1

© 2021 American Meteorological Society. For information regarding reuse of this content and general copyright information, consult the AMS Copyright Policy (www.ametsoc.org/PUBSReuseLicenses).

Brought to you by KYUSHU UNIVERSITY | Unauthenticated | Downloaded 05/13/24 03:57 AM UTC

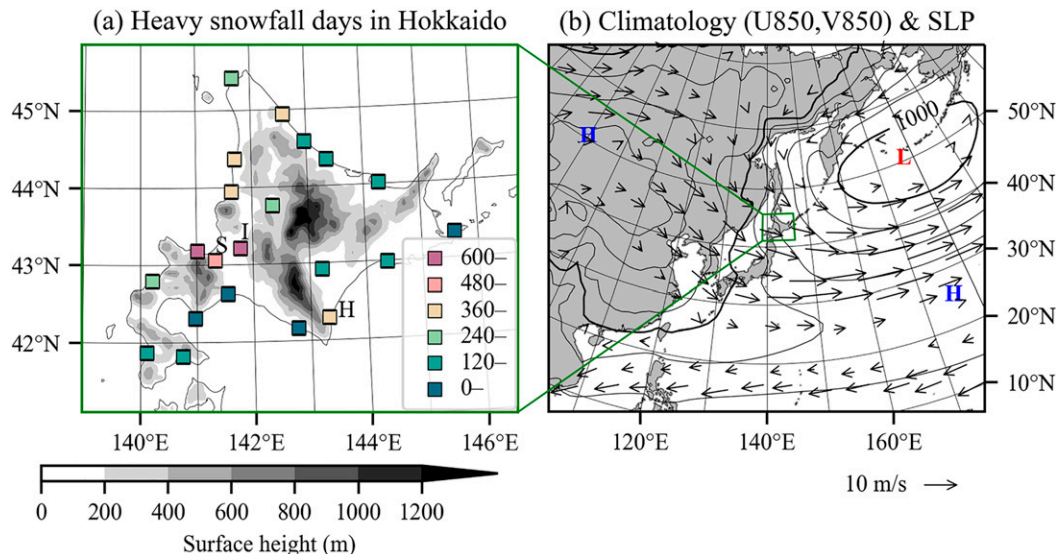


FIG. 1. (a) Heavy snowfall days in winters from 1961 to 2020 at JMA observation sites in Hokkaido. Heavy snowfall days are defined as days on which snowfall exceeds 10 mm in water equivalent. Shading denotes surface height above the sea level (m), with the key at the bottom. The observation sites Hiroo, Iwamizawa, and Sapporo are indicated by the letters H, I, and S, respectively. (b) Climatology of SLP (contours) and horizontal wind at 850 hPa (vectors) on 15 Jan of the calendar day based on JRA-55 reanalysis data from 1960 to 2019. The contour interval is 4 hPa, and contours are thickened every 20 hPa. Wind speed less than 3 m s^{-1} was masked out, and the unit vector of 10 m s^{-1} is shown at the bottom right. The marks L and H denote local SLP minimum and maximum, respectively. The green-outlined box indicates the domain of (a), including Hokkaido Island.

phenomena responsible for an attractor, or the typically unresolved environment, as stated above.

Considering the original design of the SOM, it can be also applied to the projection of the occurrence probability of unresolved phenomena. Palmer (1999) conceptually interprets the global warming response as a drift of PDF from one attractor to another on the state space. The PDF estimate of future climate data can be projected on the state space

TABLE 1. Longitude, latitude, maximum snowfall (mm day^{-1} in water equivalent) in winters from 1961 to 2020, and percentile values for snowfall of 20, 10, and 5 mm day^{-1} in water equivalent, for all AMeDAS sites analyzed in this paper (Fig. 1a).

AMeDAS site	Lon	Lat	Max (mm day^{-1})	20 mm day^{-1} (%)	10 mm day^{-1} (%)	5 mm day^{-1} (%)
Sapporo	141.328	43.060	48.5	98.854	93.884	84.187
Wakkanai	141.678	45.415	44.5	99.449	96.187	85.554
Kitami-Esashi	142.585	44.940	42.5	99.240	95.251	86.006
Haboro	141.700	44.363	59.0	99.361	94.909	81.488
Oumu	142.963	44.580	43.0	99.614	98.039	93.609
Rumoi	141.632	43.945	35.0	99.537	95.702	84.154
Asahikawa	142.372	43.757	31.0	99.791	96.749	86.501
Abashiri	144.278	44.017	75.0	99.526	97.697	92.826
Otaru	141.015	43.182	44.0	98.898	92.694	79.229
Iwamizawa	141.785	43.212	40.1	98.876	92.760	80.992
Obihiro	143.212	42.922	73.1	99.262	97.399	94.380
Kushiro	144.377	42.985	72.0	99.614	98.424	95.140
Nemuro	145.585	43.330	35.5	99.791	98.711	96.209
Suttsu	140.223	42.795	35.3	99.713	96.474	84.507
Muroran	140.975	42.312	32.5	99.791	98.700	95.405
Tomakomai	141.547	42.623	41.5	99.780	98.898	95.956
Urakawa	142.777	42.162	24.3	99.978	99.317	96.705
Esashi	140.123	41.867	39.5	99.857	98.358	91.328
Hakodate	140.753	41.817	37.0	99.857	98.567	92.705
Kucchan	140.757	42.900	49.5	97.774	84.650	67.372
Monbetsu	143.355	44.345	46.5	99.603	98.094	94.105
Hiroo	143.317	42.293	86.3	98.402	95.526	91.218

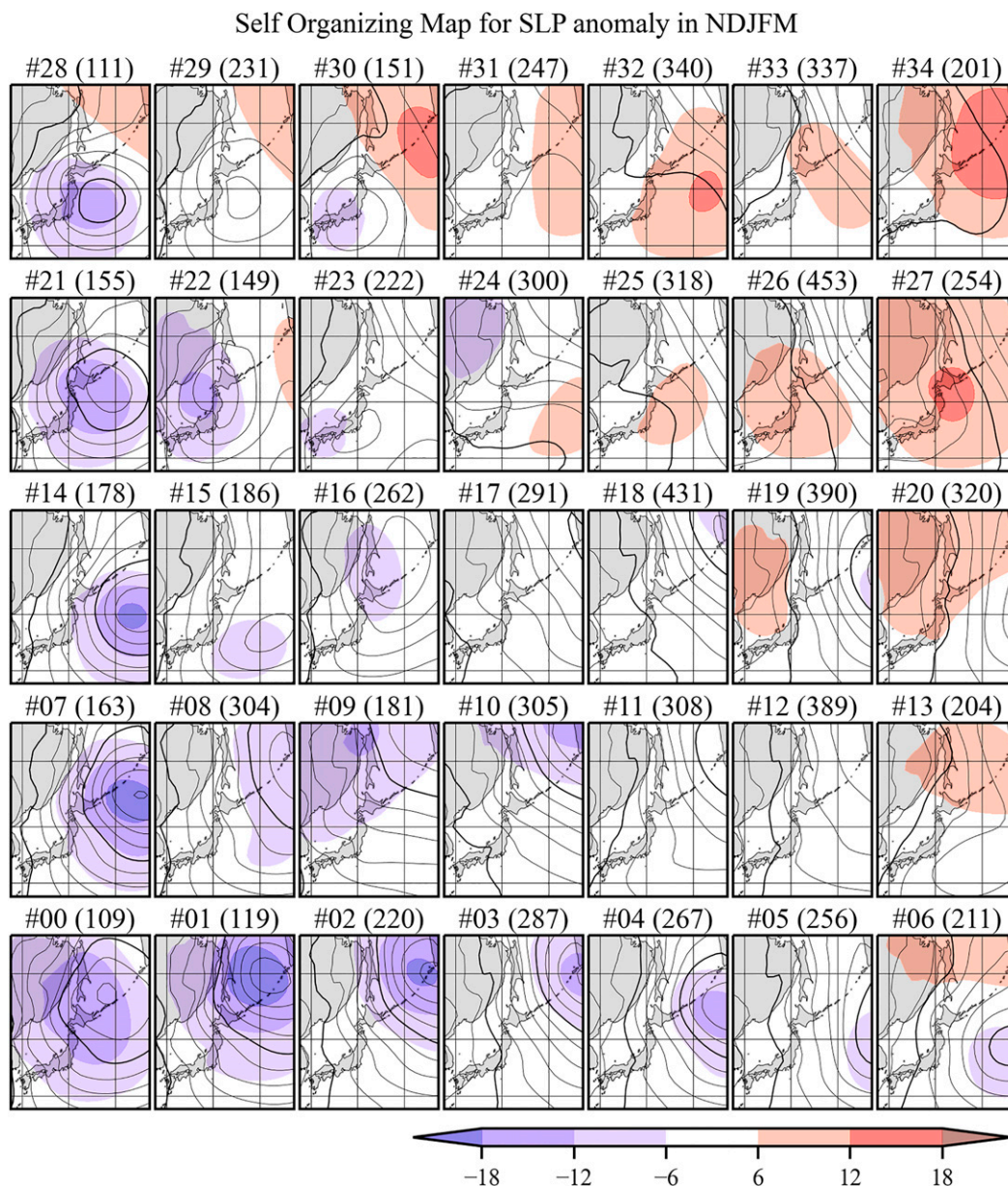


FIG. 2. SOM classification based on 6-hourly data in winter days from 1960/61 to 2019/20. Color shading shows SLP anomaly, with the key at the bottom. Contours show SLP anomaly added with the climatology of the calendar date of 15 Jan. The number of days classified into the node is indicated at the top of each plot; this is computed by the data at 0000 UTC of 150 days after 1 Nov 1960–2019. The SOM was computed for the domain of 27.5°–55°N and 127.5°–157.5°E shown here.

spanned by the bases representing present-climate variability. It is likely equivalent to the probability calculation of future climate data projected on the SOM nodes created from present-climate training data (Ohba 2019; Ohba et al. 2016). This is in contrast to SOMs trained using a combination of present and future climate-simulation datasets (Cassano et al. 2007; Schuenemann and Cassano 2010; Ohba and Sugimoto 2020; Kawazoe et al. 2020). In Hokkaido, Kawazoe et al. (2020) showed that future changes in snowfall associated with weather

patterns producing cold advection increases in frequency/intensity when below the freezing point, whereas another cluster related to warm advection decreases the chance due to melting of ice/snow above the freezing point.

The purpose of this study is to show potential use of SOMs' projection in the environment where the synoptic-scale environment strongly controls local-scale precipitation, as an extension of Kawazoe et al. (2020). Here we will extend the analysis of recent trend detected from the historical data, which

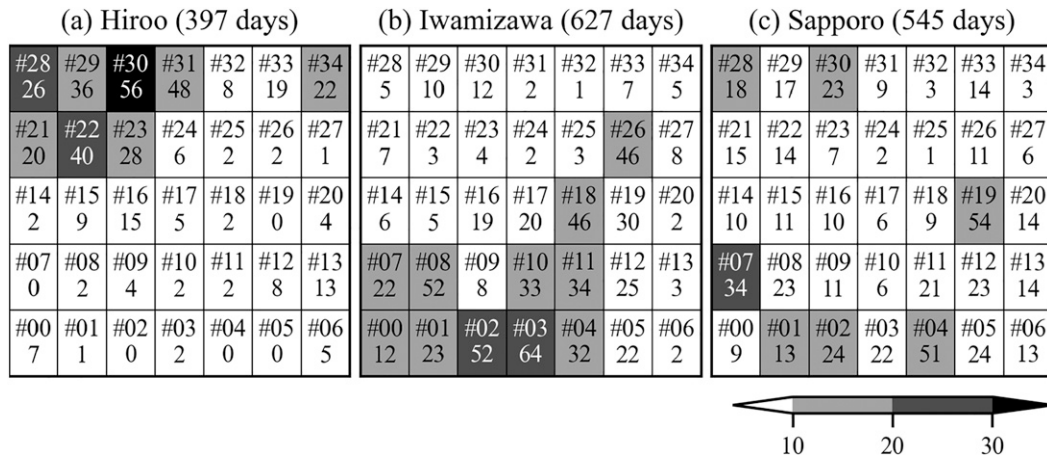


FIG. 3. Heavy snowfall days projected onto the SOM nodes at (a) Hiroo, (b) Iwamizawa, and (c) Sapporo in 150 winter days from 1961/62 to 2019/20. The heavy snowfall rate (%) in the nodes is shaded as per the key at the bottom right.

should be examined in parallel to global warming response in future projections. We expect that a close relationship between surface wind and heavy snowfall area in Hokkaido, shown by many studies, enables us to explore the heavy snowfall distribution in the future climates. Again, the heavy snowfall day is defined as the day when the snowfall exceeds 10 mm in water equivalent in this paper, but if one doubled or halved this threshold, the overall results would not change qualitatively.

2. Data and method

a. Data

Sea level pressure (SLP) anomalies from the 6-hourly Japanese 55-year Reanalysis data (JRA-55; Kobayashi et al. 2015) for 150 annual winter days from 1 November for the years 1960 to 2019 are used for SOM and its trend analysis. We used $1.25^\circ \times 1.25^\circ$ gridded data that were originally computed with the TL319 resolution and 60 vertical levels. We computed the 6-hourly climatology over the period from 1960 to 2020 and created 6-hourly anomaly as the difference between the original data and the climatology. Composite analyses were constructed using JRA-55 data for zonal and meridional winds, air temperatures at 850 hPa, and for geopotential height at 500 hPa. To associate synoptic patterns to observed snowfall in Hokkaido, we used daily accumulated precipitation, 2-m air temperature, and 2-m relative humidity observed at 21 Automated Meteorological Data Acquisition System (AMeDAS) stations in Hokkaido (Fig. 1a), operated by the JMA, from 1961 to 2020. Hourly precipitation was regarded as snow if relative humidity (%) is below $-7.5T + 93$, where T denotes surface air temperature ($^\circ\text{C}$); it is otherwise rain (Matsuo et al. 1981). Daily snowfall is the sum of hourly snowfall based on this formula.

The trend of snowfall and SOM frequency over the recent 60 years was calculated using the linear regression analysis. The statistical significance was tested by the t value of linear

trend divided by the standard error. To link synoptic patterns to snowfall, historical and +4-K simulations of d4PDF dataset were also used for comparison. The model used in the d4PDF was the Meteorological Research Institute's atmospheric general circulation model, version 3.2, with 60-km resolution. The historical simulation consisted of 100 members of an ensemble integration driven by the historical external forcing, such as greenhouse gases, and historical sea surface temperatures (SSTs) and sea ice concentration from 1951 to 2010 (Hirahara et al. 2014). The +4-K simulation consisted of total 90 members of ensemble with 15 integrations under six different SSTs; climatological SST warming patterns from six models from phase 5 of the Coupled Model Intercomparison Project (CMIP5) were added to the detrended observed SST time series. The greenhouse gases at the value of 2090 of representative concentration pathway 8.5 designed in CMIP5 were given throughout the 60-yr integration and each pattern was multiplied by a scaling factor so as to give a global-mean surface air temperature warming of 4 K. Four models represented El Niño-like patterns in climatological SST response to global warming, whereas others represented more zonal SSTs in the tropics (Mizuta et al. 2017). As Kawazoe et al. (2020) did not show notable differences in heavy snowfall characteristics among the six CMIP5 SST patterns, hereinafter all 90 members were combined to represent the +4-K simulation, unless otherwise noted. Dynamical downscaling to 20 km for historical and +4-K simulations of d4PDF was used to diagnose heavy snowfall difference between future and historical climates.

b. Self-organizing map

For the SOM computation used in this study, we followed the method outlined by Tanji et al. (2021), which adopted from Kawazoe et al. (2020). The SOM algorithm was trained on a 6-hourly SLP anomaly from a domain covering $27.5^\circ\text{--}55^\circ\text{N}$ by $127.5^\circ\text{--}157.5^\circ\text{E}$ and projected onto a 7×5 node map. Assuming that the time scale of synoptic-scale atmospheric circulation is 5 days in the target domain, this choice of the

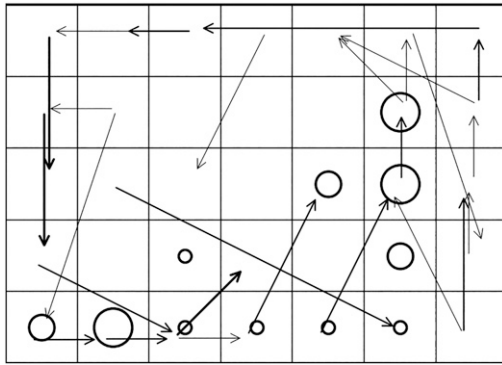


FIG. 4. One-day node-to-node transition map with the thin, standard, and thick arrows denoting the transition probability exceeding 0.15, 0.2, and 0.25, respectively. Small, medium, and large circles respectively show that the probability with no transition in a day exceeded 0.15, 0.2, and 0.25.

SOM-node number allowed us to examine heavy snowfall days from ~ 50 independent synoptic samples in each node when we were based on 150 days in 60 winters. We used a traditional SOM algorithm with the Euclidean distance searching for the best matching unit. Twenty principal components of 6-hourly SLP anomaly for the domain, which explained 98.67% of total variance, was used as input for the SOM algorithm for reduction of computation. The SLP anomaly in each SOM node was reconstructed from 20 principal components, and the reference SOM map was obtained (Fig. 2). The SOM map was made based on JRA-55 analysis, and it was also used in the analysis for historical and +4-K simulations of d4PDF as the reference SOM map.

3. Results

a. SOM and heavy snowfall

The reference SOM map in this paper (Fig. 2) was very similar to that in Kawazoe et al. (2020): Patterns included negative SLP anomalies in the east or southeast of the Hokkaido Island (top left of map), strong positive SLP anomalies over the Okhotsk sea (top right), strong negative SLP anomalies over Hokkaido and the Okhotsk Sea (bottom left), moderate positive anomalies in the north, and negative anomalies in the southeast (bottom right).

According to SOM maps that we obtained (Fig. 2), the monsoonal wind direction and its accompanied snowfall depended on the position of the cyclonic anomaly near Hokkaido. A cyclone to the south of Hokkaido brought southeasterly wind, which favors heavy snowfall in the southern part of Hokkaido, including Hiroo (H label in Fig. 1a). A cyclone in the east of Hokkaido instead brought westerly to northerly winds, which favor heavy snowfall in the western part of Hokkaido. The latter case can be separated into two patterns, one where the wind direction is west to northwest, and the other with winds northwest to north. Snowfall was often heavy in Iwamizawa (I in Fig. 1a) in

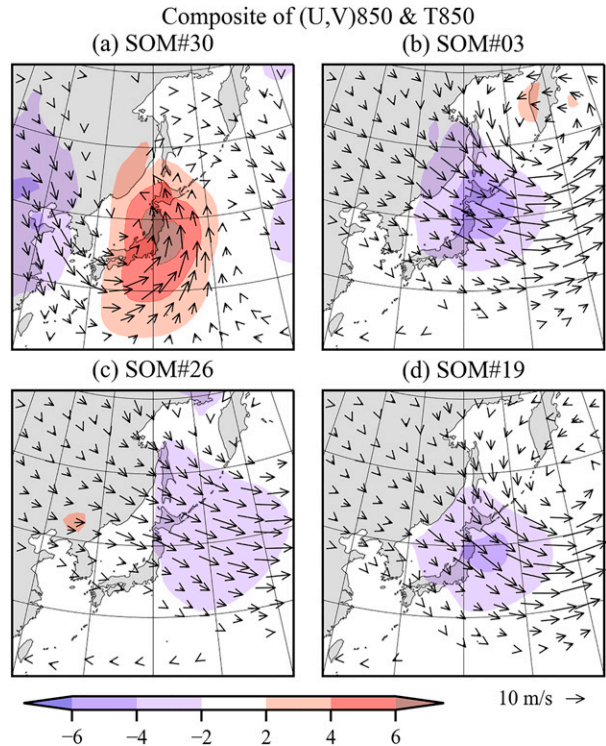


FIG. 5. Air temperature anomaly (K; color shading) and horizontal wind vector at 850 hPa (vectors), composited for days categorized into SOMs (a) 30, (b) 3, (c) 26, and (d) 19. Color shading is as per the key at the bottom left. Wind speed less than 0.5 m s^{-1} was masked out, and a unit vector of 10 m s^{-1} is shown at the bottom right.

the case of westerly to northwesterly, and snowfall tended to be observed in Sapporo (S in Fig. 1a) when winds were more northerly. We now focus on these three observation sites to investigate preferred weather patterns to heavy snowfall (Fig. 3).

Weather patterns that result in heavy snowfall in Hiroo are found in the seven SOM nodes located in the upper left of our SOM map (Fig. 3a). For example, more than 30% of winter days in SOM 30 were days when the snowfall exceeded 10 mm. The composite map of SOM 30 showed a typical weather pattern of an extratropical cyclone passing over central Japan (Fig. 2). It is noted that the cyclone tended to move eastward as indicated by the node-to-node transition graph (Fig. 4): the state changed from SOM 30 to SOM 29 with more than 20% probability in a day. On the front side of the cyclone, southerly wind transported warm and moist air from the south, crossing the high temperature gradient of the wintertime basic state (Fig. 5a). In days when Hiroo experienced southeasterly winds from the cyclone, orographic precipitation was likely induced by an uplift of the warm and moist air along the windward side of the mountains west of Hiroo (Fig. 1a). Hence, heavy snowfall in Hiroo strongly depended on the passage of extratropical cyclones. The fewer number of heavy snowfall days was related to the observed

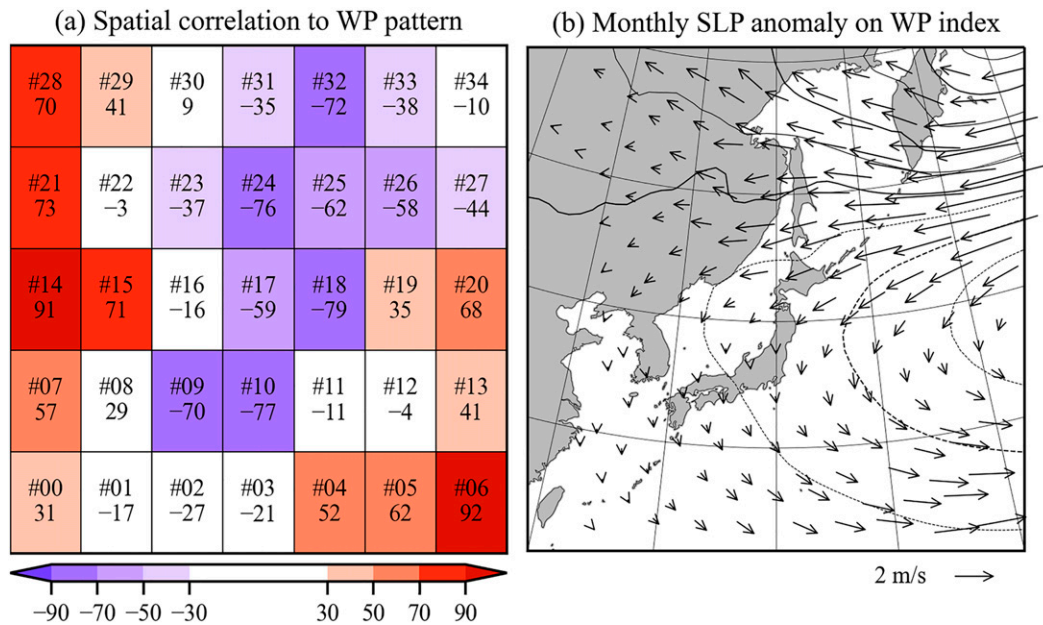


FIG. 6. (a) Spatial correlation between SLP anomaly of each SOM node and monthly SLP anomaly regressed on the monthly WP index. The color shading shows the percentage of correlation as per the key at the bottom. (b) SLP (contours) and 850-hPa horizontal wind (vectors), regressed on the WP index based on monthly mean data. The contour interval is 1 hPa; negative contours are dashed. Wind speed less than 0.5 m s^{-1} was masked out, and the unit vector of 2 m s^{-1} is shown at the bottom right.

evidence that snowfall in Hiroo was an intermittent phenomenon caused by transient eddies.

Heavy snowfall in Iwamizawa, in contrast, preferred weather patterns found in SOMs 2, 3, 8, 10, 11, 18, and 26 (Fig. 3b). SOMs 10, 18, and 26 were located near to climatological state (Fig. 1b) and had moderate westerly to northwesterly winds over Hokkaido, whereas SOMs 2, 3, and 8 were characterized by the low pressure anomaly located in Okhotsk Sea near the Kamchatka Peninsula, and strong westerly to northwesterly were observed especially in western Hokkaido (Fig. 2). Both patterns corresponded to cold-air advection from the northwest (Figs. 5b,c). More than 20% of days fallen into SOMs 2 and 3 were days when the snowfall exceeded 10 mm in Iwamizawa. The composite map of SOMs 3 and 26 showed a typical weather pattern sandwiched between the Siberian high and the Aleutian low, which had persistency in a time scale of a week or longer (Figs. 5b,c). The greater number of heavy snowfall days relative to Hiroo was indeed related to this persistent weather pattern, which was indicated by no transition from SOMs 0, 1, 18, 19, and 26 within a day with more than 20% probability (Fig. 4).

Partly as suggested in Kawazoe et al. (2020), heavy snowfall in Sapporo frequently occurred in three possible weather patterns: a passage of extratropical cyclones in the south of Hokkaido (SOMs 28 and 30), a pressure pattern between the Siberian high and the Aleutian low (SOMs 1, 2, and 7), and a weather pattern with a low pressure anomaly just in the east of Hokkaido (SOMs 4 and 19). The first and second SOM groups were associated with heavy snowfall in Hiroo

and Iwamizawa, respectively. The composite map for SOM 19 (Fig. 5d) was very similar to that for SOM 3 (Fig. 5b), but the center of action of low pressure in SOM 19 was located just east of Hokkaido and slightly shifted to the south in comparison with low pressure in SOM 3. The difference in the position of the cyclone center was very slight, but the wind direction around Hokkaido was notably different. SOM 19 showed northwesterly to northerly winds, whereas SOM 3 showed westerly to northwesterly winds.

We remark that the SOM map was closely related to the western Pacific (WP) pattern (Fig. 6b) with a dipole anomaly pattern in the western North Pacific. The index was defined as

$$\frac{1}{\sqrt{2}} [Z_{500}^*(60^\circ\text{N}, 155.25^\circ\text{E}) - Z_{500}^*(30^\circ\text{N}, 155.25^\circ\text{E})], \quad (1)$$

slightly modified from Wallace and Gutzler (1981), where Z_{500}^* denotes the normalized geopotential height anomaly at 500 hPa from the JRA-55 data. Moreover, the spatial correlation between SOM-node and WP patterns contrasted negative values from the upper right to the bottom left and positive values in the upper left and the bottom right (Fig. 6a). This suggested that the WP pattern controlled the geographical pattern of heavy snowfall in Hokkaido via prevailing wind direction associated with the weather pattern: negative WP-induced westerly winds (Fig. 6b).

Referring to the SOM map (Fig. 2), it can be summarized that the groups in the upper left, in the bottom right, and from center to bottom left were typical weather patterns associated

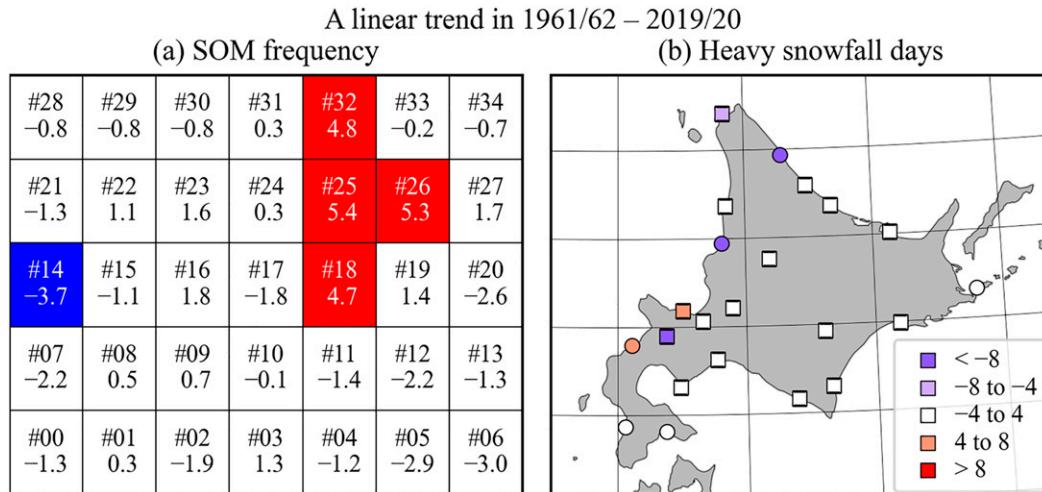


FIG. 7. (a) The linear trend of annual days classified into each SOM node $[(100 \text{ yr})^{-1}]$. Colored nodes showed the statistically significant trend ($p < 0.05$). (b) The linear trend of annual heavy snowfall days $[(100 \text{ yr})^{-1}]$ at observation sites in Hokkaido. Circles denote statically significant signal ($p < 0.05$).

with heavy snowfall in Hiroo, Sapporo, and Iwamizawa, respectively. Hereinafter we define group 1 as SOMs 21, 22, 23, 28, 29, 30, and 31; group 2 as SOMs 2, 3, 8, 10, 11, 18 and 26; and group 3 as SOMs 4, 5, 6, 12, 13, 19, and 20. We will relate these SOM-node groups to recent linear trends and global warming response.

b. Linear trend

The linear trend of the number of days fallen into each SOM node is shown in Fig. 7. Because the midlatitude winter had large interannual variability, we could not detect a statistically significant ($p < 0.05$) signal in most of the nodes (Fig. 7a). Out of all signals, only SOMs 18, 25, 26, and 32 had a positive linear trend of nearly 5 days $(100 \text{ yr})^{-1}$ in the winter season. Since the seasonal-mean days that fell into these SOM nodes were 5–7 days (Fig. 2), the number of days increased by 45%–90% in the last 60 years. Even the grouping of SOMs did not always make the signal of significant linear trend detectable. The linear trend of groups 1, 2, and 3 is -0.7 , 8.5 , and $-11.8 (100 \text{ yr})^{-1}$, respectively (Figs. 8b–d), but only the signal for group 3 is statistically significant ($p < 0.05$). Only a few points at Suttsu, Rumoi, and Kitami-Esashi (Table 1) showed statistically significant signals in the linear trend of heavy snowfall days (Fig. 7b).

The time series of the number of days classified into groups 1, 2, or 3 contained larger interannual variability, and this likely caused the statistical insignificance of the linear trend of groups 1 and 2. The historical simulation of d4PDF has 100 members, and if we take the ensemble mean, the interannual variability can be largely reduced (Figs. 8b–d). The linear trends of the SOM number fallen into group 1, 2, and group 3 were 1.7 , 4.1 , and $-6.8 (100 \text{ yr})^{-1}$, based on the ensemble-mean time series of the historical simulation (Figs. 8b–d). Although the SOM frequency in the historical simulation was overestimated for SOMs 3, 4, 19, 26, and 27 and underestimated for SOMs 17, 24,

and 25 (Fig. 8a), the linear trends for groups 2 and 3 were statistically significant ($p < 0.05$). The decreasing trend for group 3 was common in historical simulation and in JRA-55 analysis.

c. Global warming response

Though the signal of observed and simulated linear trends was rather obscure, the global warming response from model large-ensemble simulations are much clearer. The difference between +4-K and historical simulation of d4PDF was statistically significant ($p < 0.05$) for all nodes except for 21 and 31. The frequency of days in SOM group 2 increased, while those in group 3 decreased (Fig. 9a), which is consistent with the linear trend analysis in section 3b (Figs. 8b–d). The increasing nodes corresponded to a high occurrence of heavy snowfall in Iwamizawa (Fig. 3b). The decreasing nodes corresponded to the third typical pattern that brought heavy snowfall in Sapporo by northerly winds (Figs. 3c, 5d). We also indicated, with a less clear signal, a decreasing frequency in group 1 related to the passage of extratropical cyclones (Fig. 9a).

The global warming response showed a dipole pattern in the east of 145°E with cyclone anomaly in the north and anticyclonic anomaly in the south (Fig. 9b), which was correlated with SOMs 10 and 18 and anticorrelated with SOMs 6 and 14.¹ This global warming response showed an anticorrelated relationship when compared with the WP pattern (Fig. 6b), with its spatial correlation of -0.90 . The WP pattern in the upper troposphere had a center of action in the southwest when compared with the SLP signal, likely related to the temperature contrast between land

¹ This is not dependent upon the global warming response of SST distribution, except that the simulation with MIROC's SST projection provided the SLP anomaly shifted northward in comparison with the others (not shown).

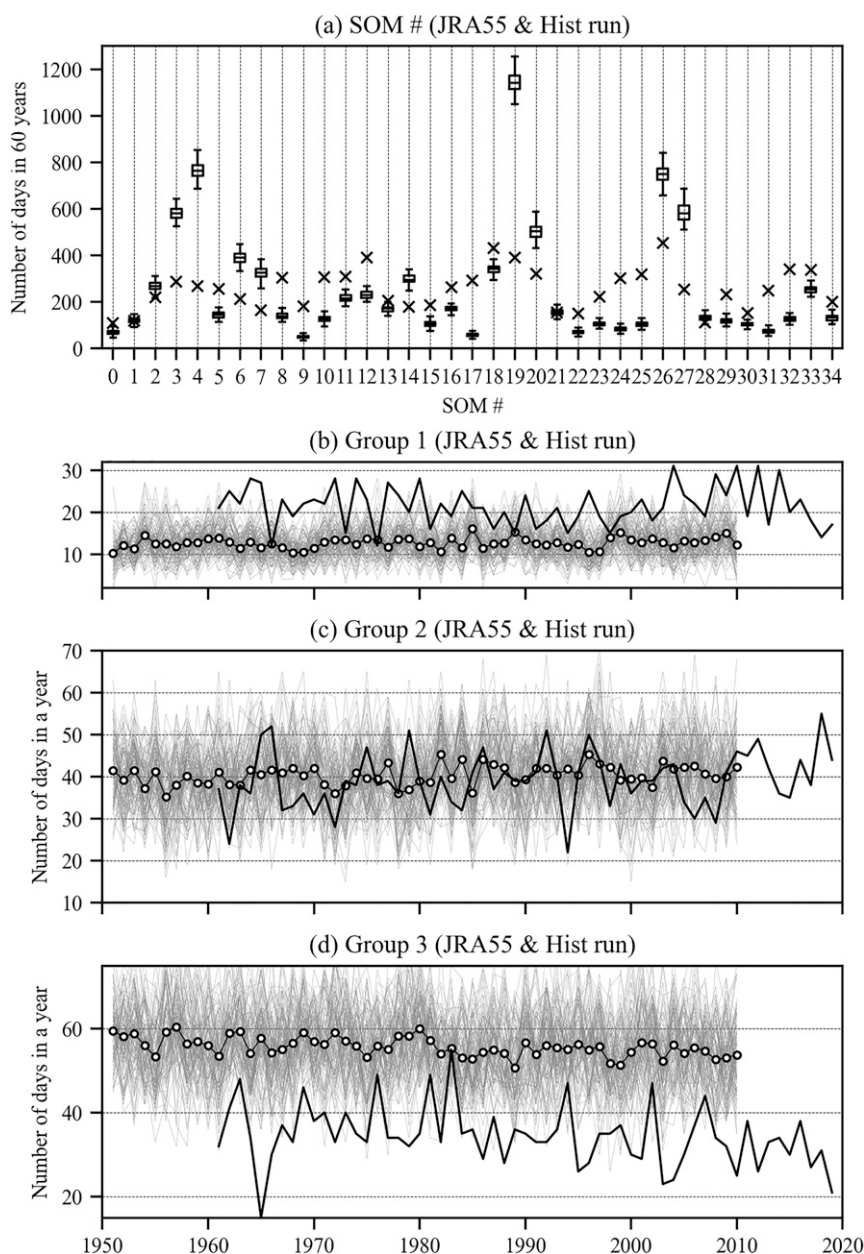


FIG. 8. (a) Number of days $[(60 \text{ yr})^{-1}]$ classified into each SOM node for JRA-55 analysis (crosses) and d4PDF's historical simulation (box-and-whisker plot that shows median, upper and lower quartiles, minimum, and maximum). Also shown is number of days (per year) in (b) group 1, (c) group 2, and (d) group 3 of SOMs for JRA-55 analysis from 1960/61 to 2018/19 (solid line) and each ensemble of 100 historical simulations from 1950/51 to 2009/10 (gray lines). The thin line with circles denotes the ensemble average of the historical simulations.

and ocean (Tanaka et al. 2016). Presumably because global warming would weaken the contrast, the negative phase of the WP pattern might emerge as the global warming response.

The dynamical downscaling results in d4PDF showed a significant decrease in total snowfall amount except for a mountainous area in central Hokkaido (Fig. 9c), similar to climate change response shown in Katsuyama et al. (2020). It is noted that the signal was statistically significant ($p < 0.05$) over most areas.

The amount decreased approximately by 50% in the coastal region in Hokkaido and the decreasing ratio was larger in the southern side. However, heavy snowfall days showed either a negligible change or increased in central Hokkaido, including Iwamizawa. This was contrasted with Hiroo, where it decreased by 70% in the +4-K simulation. In midwinter, the heavy snowfall days in Iwamizawa increased by $\sim 50\%$, whereas that in Hiroo decreased by $\sim 70\%$ (Fig. 9d).

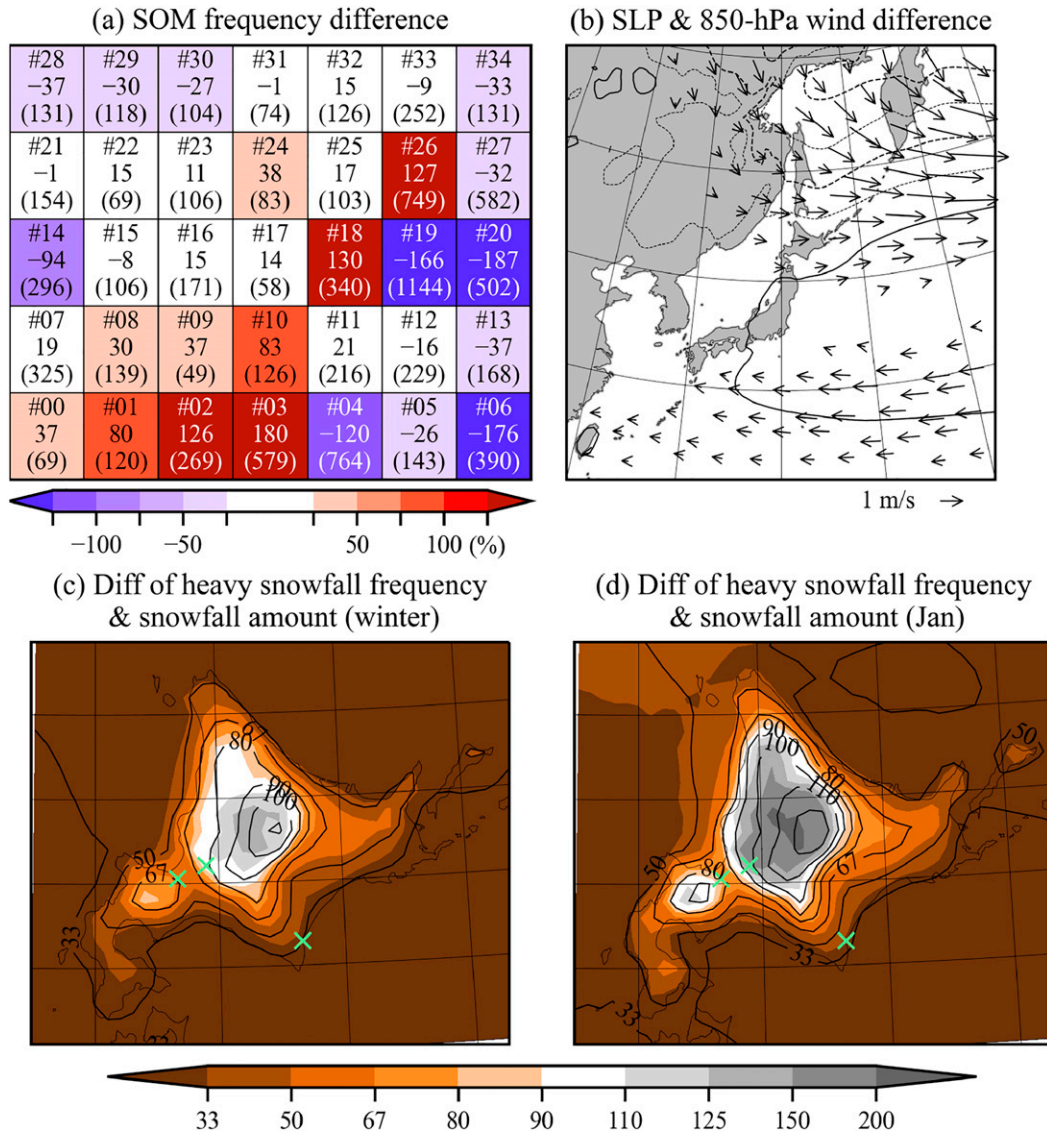


FIG. 9. (a) Difference of the number of days classified into each SOM node difference between +4-K and historical 60-yr simulations. The historical simulation has 100 members, and the +4-K simulation has 90 members. The bottom line (in parentheses) of each box shows the number of days classified into each SOM node in historical 60-yr simulations (per member). The SOM nodes are colored for the number as per the key under the panel. The difference is statistically significant ($p < 0.05$) for all nodes except for 21 and 31. (b) Difference of SLP (hPa; contours) and 850-hPa horizontal wind (vectors) between plus 4-K and historical 60-yr simulations. The contour interval is 1 hPa. Wind speed less than 0.5 m s^{-1} was masked out, and the unit vector of 1 m s^{-1} is shown at the bottom right. (c) The ratio of heavy snowfall day frequency (contours) and the ratio of total snowfall amount (shading) in the historical simulation to those in the +4-K simulation for all winter days. Light-green crosses indicate (from west to east) the Sapporo, Iwamizawa, and Hiroo stations. (d) As in (c), but the analysis is limited to days in January.

A composite map of the snowfall amount for three groups of SOM nodes (defined in section 3a) by using d4PDF simulation is shown in Figs. 10a–c. Consistent with the analysis for observation, heavy snowfall in the western side is strongly related to group 2 (westerly dominated monsoon patterns) and those in the southern and eastern side is related to group 1 (southern passage cyclone patterns). Group 3 showed an

intermediate feature between group 1 and group 2. The difference between +4-K and historical simulation showed a clear contrast between groups 1 and 2 (Figs. 10d–f). We found the decrease in snowfall or heavy snowfall days over Hokkaido in the composite for group 1. This is related to the fact that the snowfall in group 1 occurred under the environment of warm air advection by an extratropical cyclone passing to the south

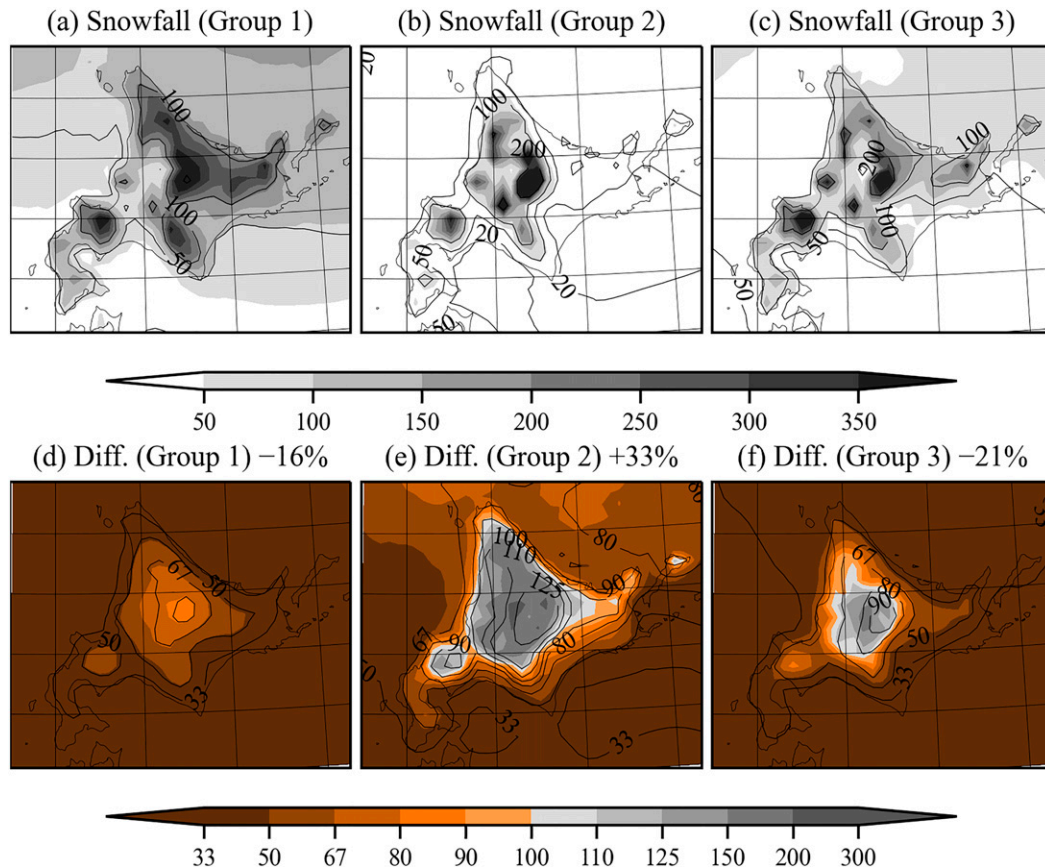


FIG. 10. Total snowfall amount in winter season (mm per season in water equivalent; contours) and total heavy snowfall days in 60 years (shading) under the historical simulation for (a) group 1, (b) group 2, and (c) group 3. The shading is as per the key at the bottom of (a)–(c). (d)–(f) As in (a)–(c), but for the ratio of +4-K simulation result to historical simulation result (%). The SOM frequency difference is shown in the title of each panel.

of Hokkaido Island. Global warming decreased the number of days when surface temperatures were favorable for snowfall. Group-1 frequency decreased by 16% in +4-K simulation. We now compute snowfall amount as a function of surface air temperatures for group 1 (Fig. 11b). The snowfall in Hiroo was simulated in the range between -5° and 5°C under the synoptic weather pattern fallen into group 1 (Fig. 11b). The temperature increase of $\sim 5\text{ K}$ resulted in fewer snow events, because there are higher number of days where surface air temperature exceeded the freezing point. The decrease in heavy snowfall days in Hiroo can then be explained by the combined effect of snow melting under a warmer environment and a slight decrease of circulation patterns that results in heavy snowfall.

There is an increase in snowfall or heavy snowfall days in Iwamizawa in central Hokkaido in the composite for group 2 (Fig. 11a). This is related to the fact that the snowfall in group 2 occurred under the environment of cold-air advection by winter monsoon. In group 2, the snowfall was simulated in the range between -15° and 0°C . Hence, global warming maintained a sufficiently low temperature condition for snowfall in central Hokkaido. The effect of cloud bands containing much more evaporation on higher SST above the freezing point of salty

water; Plus-4-K simulation was imposed a 2–3 K increase in SSTs of the Sea of Japan and 15%–20% increase in evaporation was possible. In the global warming climate, the snowfall in Iwamizawa frequently occurred under the synoptic weather patterns in group 2. Despite the temperature increase by $\sim 5\text{ K}$, the snowfall was still possible in the temperature range between -10° and 5°C . Moreover, group-2 frequency increased by 33% in +4-K simulation. The heavy snowfall days in Iwamizawa increased in the global warming climate because of the increase in water vapor capacity in the air and the increase in frequency fallen into the SOM nodes.

4. Summary

This paper showed the frequency of local-scale heavy snowfall, its long-term trend, and possible future response to global warming projected onto the SOM map of synoptic-scale weather pattern created based on SLP anomaly around Hokkaido on winter days. Since the SOM map reduced the dimension representing the state and relocated the uniform mesh to emphasize attractors on the phase space, the SOM map is effective in extracting a close relation between synoptic-scale atmospheric environment and local-scale precipitation and in interpreting its

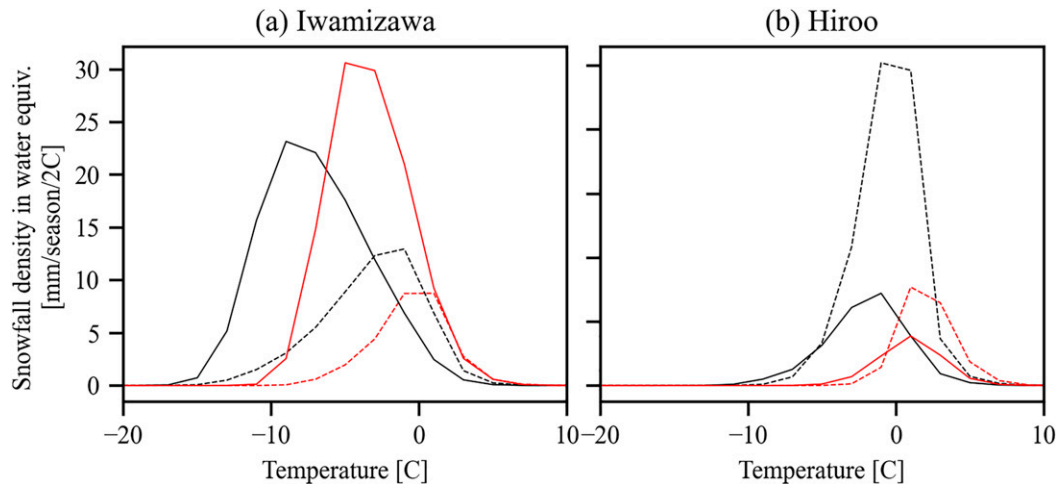


FIG. 11. Snowfall density in water equivalent (mm per season per 2°C) for the days falling into group 1 (dashed lines) and group 2 (solid lines) in (a) Iwamizawa and (b) Hiroo; the bin width in surface air temperature is 2°C . Black and red lines respectively denote the results of the HIST and +4-K runs.

phenomena. This study focused on the target domain of Hokkaido Island, whose snow climate is a great candidate for this type of study because the amount and location of snowfall are strongly tied to the synoptic weather pattern. We ascertained that the SOM map can be grouped into three categories: a passage of extratropical cyclones in the south of Hokkaido, a pressure pattern between the Siberian high and the Aleutian low, and a weather pattern with a low pressure anomaly just in the east of Hokkaido. The first and second groups were related to heavy snowfall in Hiroo and Iwamizawa, respectively, and heavy snowfall in Sapporo was related to the third group. The trend and global warming analysis revealed that the second group, related to the WP pattern, would increase in future. Heavy snowfall days in Iwamizawa would also increase as a result of the increase in water vapor and preferable weather patterns in global warming climate, in contrast to the decrease in other sites such as Hiroo, associated with SOM group 1, which are due to a warmer temperature that prohibits snowfall.

Acknowledgments. We thank the editor and three anonymous reviewers who gave us insightful comments that led to the improvement of the paper. We also thank Mr. N. Matsuoka to give us insightful comments in our earlier results. The meteorological observation, reanalysis, and forecast data were provided by the JMA. Authors Inatsu and Kawazoe are supported by the Environment Research and Technology Development Fund JPMEERF20192005 of the Environmental Restoration and Conservation Agency of Japan. Inatsu and author Mori are supported by the Integrated Research Program for Advancing Climate Models (TOUGOU) Grant JPMXD0717935457 from the Ministry of Education, Culture, Sports, Science, and Technology (MEXT). Inatsu is supported by JSPS KAKENHI Grants (18K03734, 18H03819, and 19H00963), and by the Research Field of Hokkaido Weather Forecast and Technology Development (endowed by Hokkaido Weather Technology Center Co. Ltd.). Mori is supported by JSPS KAKENHI Grants (19H01964 and 19H05703).

REFERENCES

- Campbell, L. S., W. J. Steenburgh, Y. Yamada, M. Kawashima, and Y. Fujiyoshi, 2018: Influences of orography and coastal geometry on a transverse-mode sea-effect snowstorm over Hokkaido Island, Japan. *Mon. Wea. Rev.*, **146**, 2201–2220, <https://doi.org/10.1175/MWR-D-17-0286.1>.
- Cassano, J. J., P. Uotila, A. H. Lynch, and E. N. Cassano, 2007: Predicted changes in synoptic forcing of net precipitation in large Arctic river basins during the 21st century. *J. Geophys. Res.*, **112**, G04S49, <https://doi.org/10.1029/2006JG000332>.
- Fujiyoshi, Y., K. Tsuboki, S. Satoh, and G. Wakahama, 1992: Three-dimensional radar echo structure of a snow band formed on the lee side of a mountain. *J. Meteor. Soc. Japan*, **70**, 11–24, https://doi.org/10.2151/jmsj1965.70.1_11.
- Hirahara, S., M. Ishii, and Y. Fukuda, 2014: Centennial-scale sea surface temperature analysis and its uncertainty. *J. Climate*, **27**, 57–75, <https://doi.org/10.1175/JCLI-D-12-00837.1>.
- Hoshino, T., T. J. Yamada, and H. Kawase, 2020: Evaluation for characteristics of tropical cyclone induced heavy rainfall over the sub-basins in the central Hokkaido, northern Japan by 5-km large ensemble experiments. *Atmosphere*, **11**, 435, <https://doi.org/10.3390/atmos11050435>.
- Iwao, K., M. Inatsu, and M. Kimoto, 2012: Recent changes in explosively developing extratropical cyclones over the winter northwestern Pacific. *J. Climate*, **25**, 7282–7296, <https://doi.org/10.1175/JCLI-D-11-00373.1>.
- Katsuyama, Y., M. Inatsu, and T. Shirakawa, 2020: Response of snowpack to $+2^{\circ}\text{C}$ global warming in Hokkaido, Japan. *J. Glaciol.*, **66**, 83–96, <https://doi.org/10.1017/jog.2019.85>.
- Kawazoe, S., M. Inatsu, T. J. Yamada, and T. Hoshino, 2020: Climate change impacts on heavy snowfall in Sapporo using 5-km mesh large ensemble simulations. *SOLA*, **16**, 233–239, <https://doi.org/10.2151/sola.2020-039>.
- Kobayashi, S., and Coauthors, 2015: The JRA-55 reanalysis: General specifications and basic characteristics. *J. Meteor. Soc. Japan*, **93**, 5–48, <https://doi.org/10.2151/jmsj.2015-001>.
- Kohonen, T., 1995: *Self-Organizing Maps*. Springer Series in Information Sciences, Vol. 30, Springer, 502 pp.
- Lindzen, R. S., and B. Farrell, 1980: A simple approximate result for the maximum growth rate of baroclinic instabilities.

- J. Atmos. Sci.*, **37**, 1648–1654, [https://doi.org/10.1175/1520-0469\(1980\)037<1648:ASARFT>2.0.CO;2](https://doi.org/10.1175/1520-0469(1980)037<1648:ASARFT>2.0.CO;2).
- Matsuo, T., Y. Sasyo, and Y. Sato, 1981: Relationship between types of precipitation on the ground and surface meteorological elements. *J. Meteor. Soc. Japan*, **59**, 462–476, https://doi.org/10.2151/jmsj1965.59.4_462.
- Mizuta, R., and Coauthors, 2017: Over 5,000 years of ensemble future climate simulations by 60-km global and 20-km regional atmospheric models. *Bull. Amer. Meteor. Soc.*, **98**, 1383–1398, <https://doi.org/10.1175/BAMS-D-16-0099.1>.
- Ohba, M., 2019: The impact of global warming on wind energy resources and ramp events in Japan. *Atmosphere*, **10**, 265, <https://doi.org/10.3390/atmos10050265>.
- , and S. Sugimoto, 2020: Impacts of climate change on heavy wet snowfall in Japan. *Climate Dyn.*, **54**, 3151–3164, <https://doi.org/10.1007/s00382-020-05163-z>.
- , D. Nohara, and Y. Toyoda, 2016: Rainfall downscaling of weekly ensemble forecasts using self-organising maps. *Tellus*, **68A**, 29293, <https://doi.org/10.3402/tellusa.v68.29293>.
- Ohtake, H., M. Kawashima, and Y. Fujiyoshi, 2009: The formation mechanism of a thick cloud band over the northern part of the Sea of Japan during cold air outbreaks. *J. Meteor. Soc. Japan*, **87**, 289–306, <https://doi.org/10.2151/jmsj.87.289>.
- Palmer, T. N., 1999: A nonlinear dynamical perspective on climate prediction. *J. Climate*, **12**, 575–591, [https://doi.org/10.1175/1520-0442\(1999\)012<0575:ANDPOC>2.0.CO;2](https://doi.org/10.1175/1520-0442(1999)012<0575:ANDPOC>2.0.CO;2).
- Sanders, F., and J. R. Gyakum, 1980: Synoptic–dynamic climatology of the “bomb.” *Mon. Wea. Rev.*, **108**, 1589–1606, [https://doi.org/10.1175/1520-0493\(1980\)108<1589:SDCOT>2.0.CO;2](https://doi.org/10.1175/1520-0493(1980)108<1589:SDCOT>2.0.CO;2).
- Schuenemann, K. C., and J. J. Cassano, 2010: Changes in synoptic weather patterns and Greenland precipitation in the 20th and 21st centuries: 2. Analysis of 21st century atmospheric changes using self-organizing maps. *J. Geophys. Res.*, **115**, D05108, <https://doi.org/10.1029/2009JD011706>.
- Tachibana, Y., 1995: A statistical study of the snowfall distribution on the Japan Sea side of Hokkaido and its relation to synoptic-scale and meso-scale environments. *J. Meteor. Soc. Japan*, **73**, 697–715, https://doi.org/10.2151/jmsj1965.73.3_697.
- Tanaka, S., K. Nishii, and H. Nakamura, 2016: Vertical structure and energetics of the western Pacific teleconnection pattern. *J. Climate*, **2**, 6597–6616, <https://doi.org/10.1175/JCLI-D-15-0549.1>.
- Tanji, S., M. Inatsu, S. Kawazoe, and Y. Sato, 2021: Blowing snow map of Hokkaido in 2017/2018 winter (in Japanese). *Seppyo*, **83**, 275–284, https://www.seppyo.org/publication/seppyo/seppyo_archives/83_2021/83_03_2021/.
- Tsuboki, K., Y. Fujiyoshi, and G. Wakahama, 1989: Doppler radar observation of convergence band cloud formed on the west coast of Hokkaido Island (2); cold front type. *J. Meteor. Soc. Japan*, **67**, 985–999, https://doi.org/10.2151/jmsj1965.67.6_985.
- Veals, P. G., W. J. Steenburgh, S. Nakai, and S. Yamaguchi, 2019: Factors affecting the inland and orographic enhancement of sea-effect precipitation in the Hokuriku Region of Japan. *Mon. Wea. Rev.*, **147**, 3121–3143, <https://doi.org/10.1175/MWR-D-19-0007.1>.
- , —, —, and —, 2020: Intrastorm variability of the inland and orographic enhancement of a sea-effect snowstorm in the Hokuriku Region of Japan. *Mon. Wea. Rev.*, **148**, 2527–2548, <https://doi.org/10.1175/MWR-D-19-0390.1>.
- Wallace, J. M., and D. S. Gutzler, 1981: Teleconnections in the geopotential height field during the Northern Hemisphere winter. *Mon. Wea. Rev.*, **109**, 784–812, [https://doi.org/10.1175/1520-0493\(1981\)109<0784:TITGHF>2.0.CO;2](https://doi.org/10.1175/1520-0493(1981)109<0784:TITGHF>2.0.CO;2).
- Yoshida, A., and Y. Asuma, 2004: Structure and environment of explosively developing extratropical cyclones in the northwestern Pacific region. *Mon. Wea. Rev.*, **132**, 1121–1142, [https://doi.org/10.1175/1520-0493\(2004\)132<1121:SAEOED>2.0.CO;2](https://doi.org/10.1175/1520-0493(2004)132<1121:SAEOED>2.0.CO;2).